Bonding in complexes of bis(pentalene)di-titanium, Ti2(C8H6)2

Article (Accepted Version)

Bonding in Complexes of Bis(pentalene)di-titanium, $Ti_2(C_8H_6)_2$.

Alexander F. R. Kilpatrick,[‡] Jennifer C. Green,*[§] and F. Geoffrey N. Cloke*[‡].

[‡]Department of Chemistry, School of Life Sciences, University of Sussex, Brighton, BN1 9QJ, UK

[§]Department of Chemistry, University of Oxford, Inorganic Chemistry Laboratory, South Parks Road, Oxford, OX1 3QR, UK

ABSTRACT

Bonding in the bis(pentalene)di-titanium 'double-sandwich' species Ti_2Pn_2 (Pn = C_8H_6) and its interaction with other fragments have been investigated by xdensity functional calculations and fragment analysis. Ti_2Pn_2 with C_{2v} symmetry has two metal-metal bonds and a low-lying metal based empty orbital, all three frontier orbitals having a_1 symmetry. The latter may be regarded as being derived by symmetric combinations of the classic three frontier orbitals of two bent bis(cyclopentadienyl) metal fragments. Electrochemical studies on $Ti_2Pn^{\dagger}_2$ ($Pn^{\dagger}$ = $C_8H_4\{Si^iPr_3\text{-}1,4\}_2$) reveal a one-electron oxidation, and the formally mixed-valence Ti(II)-Ti(III) cationic complex $[Ti_2Pn^{\dagger}_2][B(C_6F_5)_4]$ has been structurally characterised. Theory indicates an S = ½ ground state electronic configuration for the latter, confirmed by EPR spectroscopy and SQUID magnetometry.

Carbon dioxide binds symmetrically to Ti_2Pn_2 preserving C_{2v} symmetry, as does carbon disulfide. The dominant interaction in $Ti_2Pn_2CO_2$ is σ donation into the LUMO of bent CO_2 and donation from the O atoms to Ti_2Pn_2 is minimal, whereas in $Ti_2Pn_2CS_2$ there is significant interaction with the S atoms. The bridging O atom in the mono(oxo) species Ti_2Pn_2O, however, employs all three O 2p orbitals in binding and competes strongly with Pn, leading to weaker binding of the carbocyclic ligand, and the sulfur analog Ti_2Pn_2S behaves similarly.

Ti_2Pn_2 is also capable of binding one, two and three molecules of carbon monoxide. The bonding demands of a single CO molecule are incompatible with symmetric binding and an asymmetric structure is found. The dicarbonyl adduct $Ti_2Pn_2(CO)_2$ has C_s symmetry with the Ti_2Pn_2 unit acting as two MCp_2 fragments. Synthetic studies show, that in the presence of excess CO a tricarbonyl complex $Ti_2Pn^{\dagger}_2(CO)_3$ is formed, which optimises to an asymmetric structure with two terminal CO ligands and one semi-bridging. Low temperature ^{13}C NMR spectroscopy reveals a rapid dynamic exchange between the two bound CO sites and free CO.

INTRODUCTION

Pentalene (Pn = C_8H_6) and its derivatives show a variety of coordination modes to transition metals.[1] When acting as a ligand, pentalene is formally classified as a dianion, $[C_8H_6]^{2-}$, or in the CBC method (Covalent Bond Classification) as a L_3X_2 ligand.[2-4] To a certain extent its coordination chemistry resembles that of cyclooctatetraene, also a member of the L_3X_2 class, but when coordinated to a single metal in an η^8 fashion it is non-planar, folding around the two bridgehead carbons.[5-7] Much progress has been made in synthesising compounds where two metals are sandwiched between two pentalene ligands, so called 'double-sandwich' complexes. Early work by Katz employed unsubstituted pentalene forming M_2Pn_2 complexes with Co and Ni,[8,9] however, substituted pentalenes which offer solubility and steric protection have extended the number of these double sandwiches across the whole transition series.[7,10-14] Computational studies using density functional theory (DFT) have established the metal-metal bond order in these bimetallic compounds.[7,10-14] If the bridgehead carbons are treated as donating their two π electrons to both metals in a μ-L fashion, use of the 18 electron rule enables the metal-metal bond order to be predicted correctly[15] (Figure 1) and establishes that all except the Ti derivative are electronically saturated.

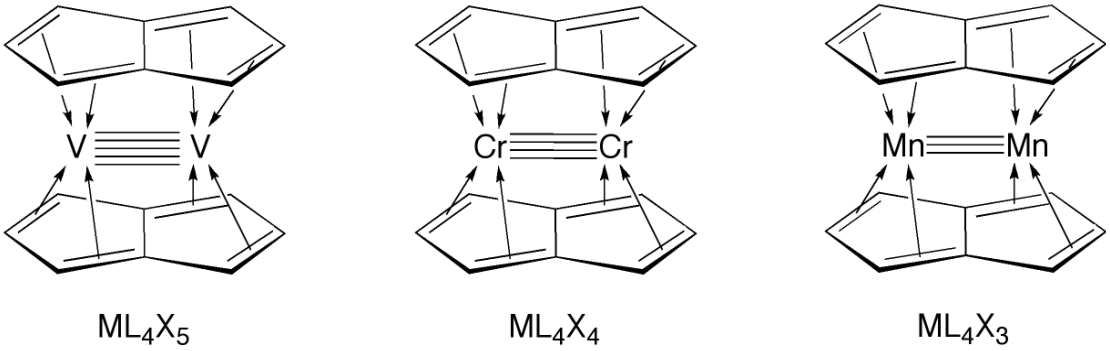

Figure 1. M–M bond orders predicted by assuming that the bridging pentalene is a 5-electron L_2X donor to each metal (bottom); the allyl portion is an LX donor. The M–M bond orders predicted are in accord with theory. Pentalene substituents are not shown for clarity.

We have recently extended the series of known bis(pentalene) double-sandwich compounds to titanium using the silylated pentalene ligand $[C_8H_4\{Si^iPr_3\text{-}1,4\}_2]$ (= $Pn^\dagger$) and $Ti_2Pn^\dagger_2$ shows unique reactivity amongst pentalene double-sandwich complexes leading to a number of novel derivatives.[16,17] The

mechanism of the reaction of its CO_2 complex is described elsewhere;[17] here we examine the bonding in a range of derivatives in more detail.

RESULTS AND DISCUSSION

All calculations employed a model system with the pentalene substituents replaced by H atoms. Key structural parameters are given in Table 1. Optimised coordinates are given in the Supporting Information (ESI). Numbers by two different computational methods are given as normal for ADF(BP/TZP) and in *italics* for Gaussian(B3LYP/SDD).

$Ti_2(\mu{:}\eta^5,\eta^5\text{-}Pn)_2$

$Ti_2(\mu{:}\eta^5,\eta^5\text{-}Pn^\dagger)_2$ has a bent structure.[14] Optimisations of the structure of $Ti_2(\mu{:}\eta^5,\eta^5\text{-}Pn)_2$ (abbreviated Ti_2Pn_2) were carried out with D_{2h} symmetry, **1**, and no symmetry constraints, **2**.

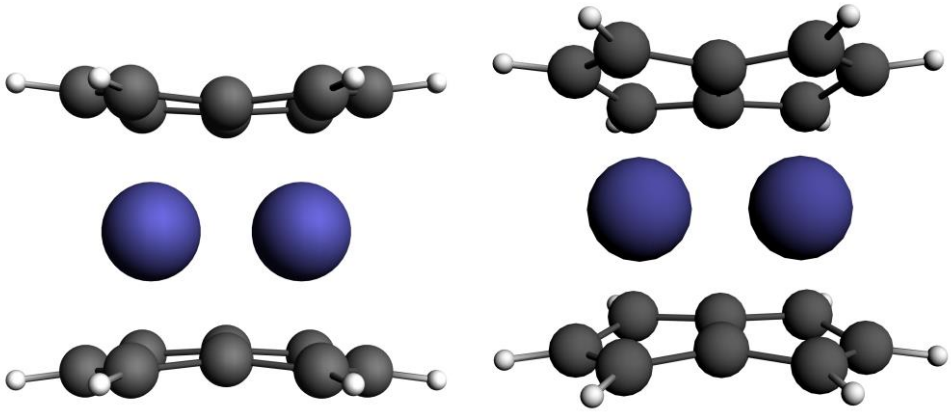

1 **2**

Structure **1** had a low imaginary frequency (wavenumber/cm^{-1}= -*i*80; -*i69*). Structure **2** had C_{2v} symmetry and was a local minimum; it was the same energy as structure **1** within computational error (*E*(**2**)-*E*(**1**)/kcal mol^{-1} = -2;+*1*). The calculated Ti-Ti distances of **2** (2.37 Å, *2.31 Å*) compare well with that found experimentally for $Ti_2Pn^\dagger_2$ (2.399(2) Å), as do the calculated centroid-metal-centroid angles (153°, *158*° calc.; 153.84(17)°, 156.6(2)° exp.) (Table 1). The short Ti-Ti distance indicates significant bonding between the Ti atoms.

Table 1. Selected calculated structural parameters (Å, °) for optimised structures. Ct denotes the η^5-centroid of the Pn ring.

Compound		Ti-Ti	Ti-Ct	Ct-Ti-Ct	Ti-C	Ti-O/S	C-O/S	O-Ti-O
Ti_2Pn_2	**1**	2.33, *2.34*	2.01, *2.01*	180, *180*				
Ti_2Pn_2	**2**	2.37, *2.31*	2.00, *2.03*	153, *158*				
$Ti_2Pn_2^+$	[**2**]$^+$	2.47, 2.43	2.03, *2.04*	145, *147*				
$Ti_2Pn_2CO_2$	**3**	2.41, *2.40*	2.07, *2.10*	141, *141*	2.18, *2.14*	2.27, *2.25*	1.26, *1.29*	
$Ti_2Pn_2CS_2$	**4**	2.43, *2.41*	2.10, *2.11*	138, *138*	2.27, *2.24*	2.54, *2.58*	1.67, *1.72*	
Ti_2Pn_2COS	**5**	2.41, *2.40*	2.08, *2.09* 2.09, *2.48*	140, *141* 139, *140*	2.19, *2.17* 2.25, *2.20*	2.19, *2.16* 2.63, *2.69*	1.26, *1.29* 1.68, *1.73*	
Ti_2Pn_2CO	**6**	2.38, *2.36*	2.06, *2.08*	143, *143*	2.04, *2.02*	2.35, *2.26*	1.21, *1.25*	
$Ti_2Pn_2(CO)_2$	**7**	2.42, *2.42*	2.05, *2.05*	144, *144* 142, *144*	2.08, *2.08*		1.17, *1.17* 1.17, *1.18*	
$Ti_2Pn_2(CO)_3$	**8**	2.63, *2.64*	2.04, *2.07* 2.09, *2.11*	143, *142* 137, *137*	2.02, *1.99* 2.06, *2.05* 2.07, *2.03*		1.17, *1.19* 1.17, *1.19* 1.16, *1.18*	
Ti_2Pn_2O	**9**	2.38, *2.36*	2.13, *2.14*	139, *140*		1.87, *1.85*		79, *79*
PnTiOTiPn S=1	**10**	3.40, *3.69*	1.96, *1.99*	57, *57*		1.86, *1.85*		133, *180*
PnTiOTiPn S=0	**11**	2.88, *2.80*	1.96, *1.99*	57, *57*		1.85, *1.83*		103, *100*
$Ti_2Pn_2O(CO)$	**12**	2.46, *2.43*	2.18, *2.17* 2.11, *2.13*	135, *137* 138, *138*	2.08, *2.07*	1.76, *1.74* 2.10, *2.07*	1.16, *1.17*	
Ti_2Pn_2S	**13**	2.44, *2.42*	2.11, *2.12*	137, 140		2.37, *2.39*		62. *61*
$Ti_2Pn_2S(CO)$	**14**	2.48	2.12 2.11	135 136	2.08	2.30 2.54		61,
$PnTiO_2TiPn$	**15**	2.74, *2.75*	2.00, *2.02*	56, *56*		1.87, *1.85*		95, *96*

The bonding in bis(pentalene)di-metal sandwiches has been discussed previously.[7,10-14,18] The bent structure of Ti_2Pn_2 introduces a new motif and small modifications to the bonding.[14] Figure 2 shows isosurfaces for the metal-based frontier orbitals for both **1** and **2**. Four electrons occupy these frontier orbitals resulting in a double bond between the Ti atoms. On lowering the symmetry from D_{2h} to C_{2v} the HOMO and HOMO-1 become the same symmetry and mix, with the consequence that the orbitals appear as two bent bonds, equivalent to a σ and a π bond. The LUMO, which is doubly occupied in the vanadium analogue,[12] is only weakly metal-metal bonding due to small overlap. The three a_1 metal-based orbitals form the principal frontier orbitals of Ti_2Pn_2. In addition the higher lying unoccupied orbitals of b symmetry are metal-metal anti-bonding and provide additional flexibility for bonding additional ligands.

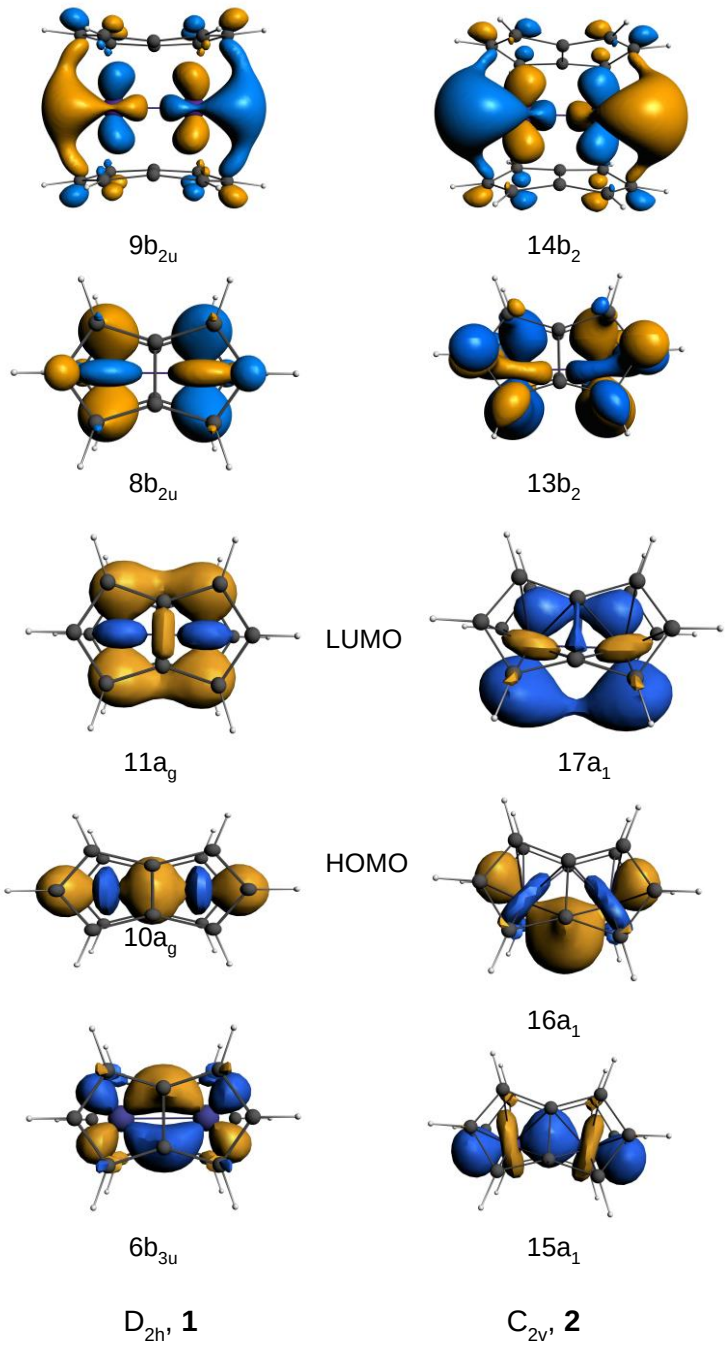

Figure 2. Frontier MOs of Ti_2Pn_2 with D_{2h}, **1**, and C_{2v}, **2**, symmetry.

The three frontier orbitals with a_1 symmetry may also be formed by in-phase combinations of the well known frontier orbitals of two bent metallocenes (Figure 3).[19-24]

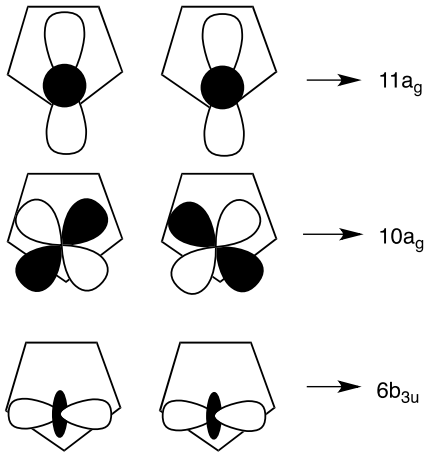

Figure 3. Derivation of frontier orbitals of Ti_2Pn_2 from those of two metallocenes.

The closeness in energy of the two structures demonstrates that there is no strong driving force towards the bent structure. Indeed, most orbitals rise marginally in energy between **1** and **2**. The one orbital that shows a significant lowering in energy is a member of the metal-ligand bonding set, shown in Figure 4. The orbitals derived from the upper occupied orbitals of the pentalene dianion, $\pi 4$ and $\pi 5$, are the principal orbitals used in metal-ligand bonding. In D_{2h} symmetry two linear combinations, $4a_u$ and $8b_{1u}$, mix well with the metal d orbitals. The other two linear combinations, $5b_{1g}$ and $9a_g$, have poor overlap with the metal set. Bending the molecule and lowering the symmetry improves the overlap for the $5b_{1g}$ orbital, which becomes the $12b_2$ orbital in C_{2v} symmetry, and it lowers in energy. This situation is reminiscent of the effect of bending in parallel metallocenes.[25]

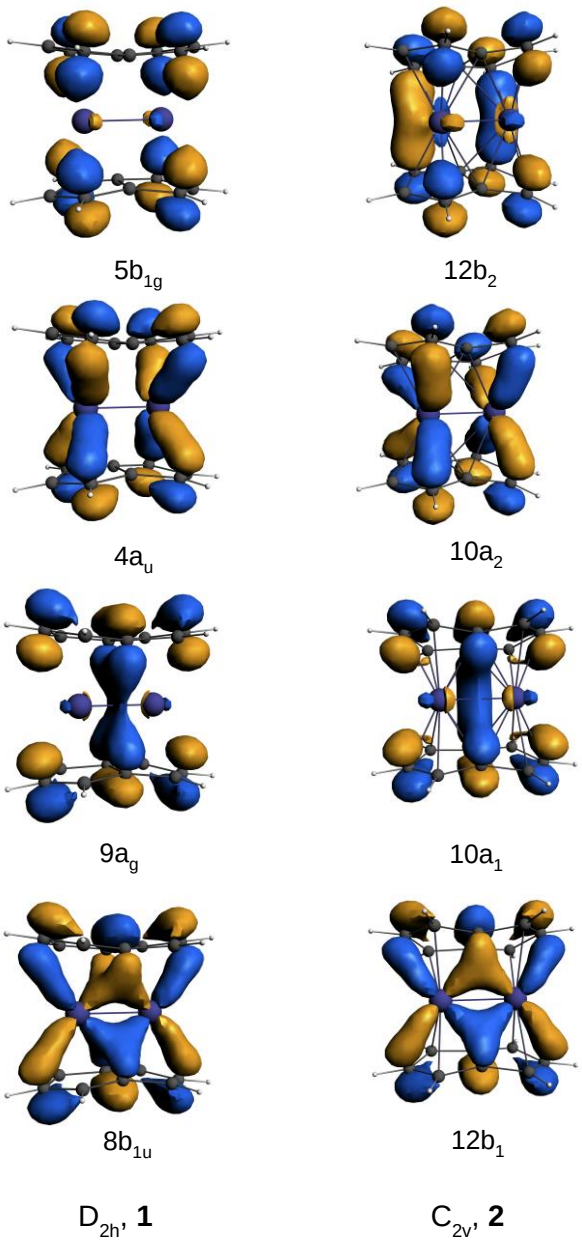

Figure 4. MOs of **1** and **2** derived from π5 and π4 of pentalene.

Electrochemical studies

Cyclic voltammetry (CV) of $Ti_2Pn^{\dagger}_2$ was carried out to assess the stability of the mixed-valence form of the bimetallic complex, and choose an appropriate chemical redox agent for its preparation on a synthetic scale.

The CV of $Ti_2Pn^{\dagger}_2$ in THF / 0.1 M [^{n}Bu$_4$N][PF$_6$] reveals two major redox processes within the electrochemical window, shown in Figure 5 with data summarised in Table 2.

Table 2. Peak potentials (E_p vs $FeCp_2^{+/0}$) and limiting currents (i_p) for the CV of $Ti_2Pn^{\dagger}_2$ in THF / 0.1 M [^{n}Bu$_4$N][PF_6], scan rate 100 mV s^{-1}.

	Process I	**Process II**
$\boldsymbol{E_{pa}}$ **/ V**	-2.38	-1.06
$\boldsymbol{E_{pc}}$ **/ V**	-2.58	-1.95
$\boldsymbol{E_{½}}$ **/ V**	-2.48	n/a
$\boldsymbol{\Delta E_{pp}}$ **/ mV**	201	893
$\boldsymbol{i_{pa}/i_{pc}}$	1.0	3.0

Process I, centred at $E_{½}$ = -2.48 V vs $FeCp_2^{+/0}$, is assigned to a reduction to the mono-anion $[Ti_2Pn^{\dagger}_2]^-$. Repetitive potential cycling over Process I in isolation using variable scan rates from 100 to 1000 mV s^{-1} (see SI), showed electrochemical behaviour best described as quasi-reversible.[26] The peak-to-peak separation (ΔE_{pp}) was similar to that for ferrocene under the same conditions (*ca.* 200 mV), suggesting that one electron is being transferred. For comparison, the permethylpentalene double-sandwich complexes $M_2Pn^*_2$ (M = V, Cr, Mn, Co, Ni; Pn* = C_6Me_6) studied by O'Hare *et al.* each show a single-electron reduction process, with electrode potentials ranging from -2.75 to -1.85 V vs $FeCp_2^{+/0}$.[12] Process II is assigned to a one electron oxidation with a peak potential (E_{pa}) of -1.06 V vs $FeCp_2^{+/0}$ in the forward scan, and an associated cathodic wave was observed at E_{pc} = -1.95 V vs $FeCp_2^{+/0}$ in the reverse scan. Irreversible behaviour suggests that the product of this oxidation $[Ti_2Pn^{\dagger}_2]^+$ is not stable under the conditions and timescale of the CV experiment. The mononuclear bis(cyclopentadienyl) titanium sandwich complexes studied by Chirik *et al.* also showed irreversible voltammetric responses in THF/[^{n}Bu$_4$N][PF_6].[27] The oxidation of double-sandwich complex $Ti_2Pn^{\dagger}_2$ occurs at a relatively cathodic potential (-1.06 V vs $FeCp_2^{+/0}$), consistent with an electron rich complex that can act as a reducing agent for substrates such as CO_2.

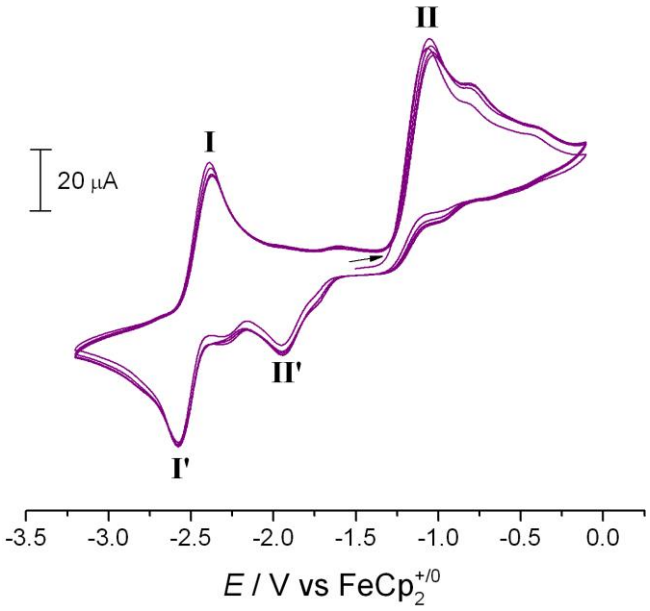

Figure 5. Overlaid CV scans (3 cycles) for $Ti_2Pn^{\dagger}_2$ in THF / 0.1 M [^{n}Bu$_4$N][PF_6], scan rate 100 mV s^{-1}.

Employing [^{n}Bu$_4$N][$B(C_6F_5)_4$] as the supporting electrolyte resulted in better resolution CV data for $Ti_2Pn^{\dagger}_2$ in oxidative scans compared with [^{n}Bu$_4$N][PF_6] (see ESI Figure S3), and a further quasi-reversible oxidation, process III, was observed at $E_{½}$ = -0.54 V vs $FeCp_2^{+/0}$. The $[B(C_6F_5)_4]^-$ anion is well-known for its lower ion-pairing capabilities (spherical diameter $[B(C_6F_5)_4]^-$ = 10 Å; $[PF_6]^-$ = 3.3 Å)[28] which are beneficial for the study of multi-electron processes with positively charged analytes,[29] and was therefore chosen for the large scale synthesis of the cationic species.

[Ti$_2$(μ:η^5,η^5-Pn†)$_2$][B(C$_6$F$_5$)$_4$]

Reaction of $Ti_2Pn^{\dagger}_2$ with the mild oxidising agent $[FeCp^*_2][B(C_6F_5)_4]$ at -35 °C resulted in a brown suspension. Following evaporation of the solvent and removal of $FeCp^*_2$, the residues were recrystallised from a concentrated Et_2O/hexane solution at -35 °C yielding $[Ti_2(\mu{:}\eta^5,\eta^5\text{-}Pn^{\dagger})_2][B(C_6F_5)_4]$ in 55% yield, which was fully characterised by spectroscopic and analytical methods. The cation $[Ti_2Pn^{\dagger}_2]^+$ is, to the best of our knowledge, the first example of a formally a Ti(II)-Ti(III) mixed-valence species. The molecular structure (Figure 6) reveals a 'naked' double-sandwich cation with no close contacts between the anion and the metal-metal bonded core.

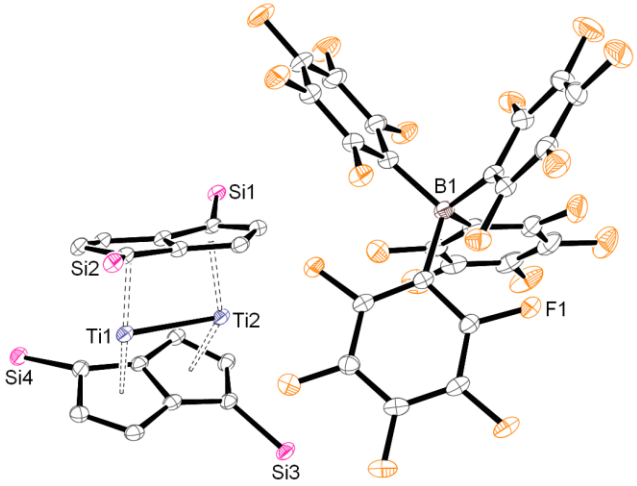

Figure 6. Displacement ellipsoid plot (30% probability) of $[Ti_2Pn^{\dagger}{}_2][B(C_6F_5)_4]$. H atoms and ^{i}Pr groups omitted for clarity. Selected structural parameters (Å, °): Ti1–Ti2 = 2.5091(9), Ti–Ct ^{a} = 2.0233(14), Ti–C_{ring} ^{a} =2.384(3), C–C_{ring} ^{a} =1.437(4), Ti1–B1 = 7.134(4), Ct–Ti–Ct ^{a} = 142.38(6), Ring slippage ^{a} = 0.105(3), Twist angle = 14.44(9), Hinge angle = 5.5(3), Fold angle = 8.38(13). Ct denotes the η^5-centroid of the Pn ring. ^{a}Average values.

The most noteworthy structural feature is the longer Ti–Ti bond distance in $[Ti_2Pn^{\dagger}{}_2][B(C_6F_5)_4]$ (2.5091(9) Å) compared with $Ti_2Pn^{\dagger}{}_2$ (2.399(2) Å). This elongation is consistent with the removal of an electron from the M−M bonding HOMO ($16a_1$) in the molecular orbital scheme for Ti_2Pn_2 (Figure 2). There is no significant difference in Ti–C and pentalene C–C bond lengths between $Ti_2Pn^{\dagger}{}_2$ and $[Ti_2Pn^{\dagger}{}_2]^{+}$, however the pentalene ligands bend around the Ti_2 core to a greater extent in the cationic complex; the centroid–metal–centroid angles around Ti1 and Ti2 are 142.28(6)° and 142.48(6)° respectively, compared with the respective angles of 153.84(17)° and 156.6(2)° in the neutral complex. The decamethyltitanocene cation in $[Cp^*{}_2Ti][BPh_4]$[30] also adopts a more bent structure than the neutral titanocenes.[31,32]

As expected $[Ti_2Pn^{\dagger}{}_2][B(C_6F_5)_4]$ is paramagnetic; the ^{1}H, ^{13}C, and ^{29}Si NMR spectra in THF-d_8 are broad and uninformative, however the ^{19}F and ^{11}B{^{1}H} NMR spectra showed well-resolved signals at δ_F -132.7, -165.2 and -168.7 and δ_B -14.75 respectively, attributable to the outer-sphere tetrakis(perfluorophenyl)borate anion. The solution phase magnetic moment of $[Ti_2Pn^{\dagger}{}_2][B(C_6F_5)_4]$ determined by the Evans method was 1.96 μ_B per dimer,[33,34] slightly greater than the spin-only moment for one unpaired electron (1.73 μ_B). Comparable data were observed in the solid state by SQUID magnetometry, μ_{eff}(260 K) = 1.92 μ_B per dimer (see SI, Figure S4).

EPR spectra of $[Ti_2Pn^{\dagger}_2][B(C_6F_5)_4]$ were consistent with an S = ½ ground state electronic configuration. The X-band spectrum of a polycrystalline sample at room temperature (Figure 7) shows an axial signal with two principal g-values simulated ($g_{\perp}$= 2.003 and $g_{\parallel}$ = 1.944), giving an average g-value of 1.964. The large linewidths ($\Delta B_{\perp}$ = 24.5 G and $\Delta B_{\parallel}$ = 23 G) meant that any hyperfine structure and further g-anisotropy were not resolved.

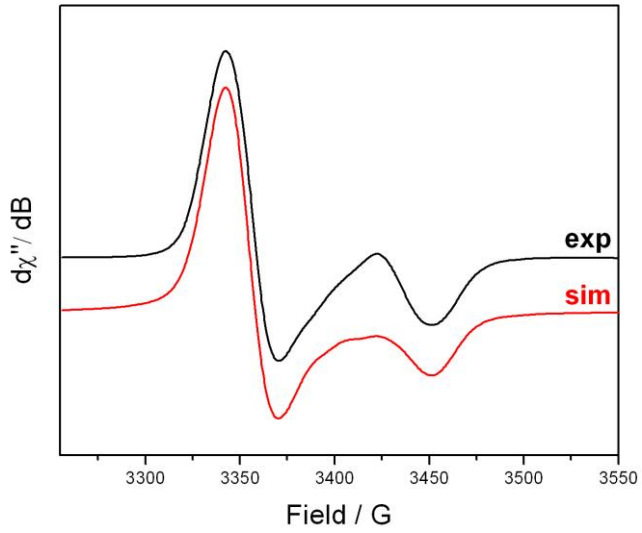

Figure 7. X-band EPR spectrum of polycrystalline $[Ti_2Pn^{\dagger}_2][B(C_6F_5)_4]$ at room temperature (black line) and corresponding simulation (red line).

$[Ti_2Pn_2]^+$

Calculations on the cation $[Ti_2Pn_2]^+$, $[\mathbf{2}]^+$, show a lengthening of the Ti-Ti distance of *ca.* 0.1 Å and an increase in the bending of the pentalene ligands around the Ti_2 core (Table 1), as found experimentally for the silylated analogues. The orbital manifold shows the expected hole in the $16a_1$ orbital (Figure 2), which is delocalised over the Ti atoms. The principal g-values calculated for $[\mathbf{2}]^+$ are g_x = 1.956, g_y = 2.000, g_z = 2.008. Their relative magnitude and ordering $g_x < g_y \approx g_z$ explains the apparent axial symmetry of the experimental EPR spectrum with the C_2 axis perpendicular to the x-axis (in a coordinate system with the x-axis passing through the pentalene bridgehead C-C bonds), and is consistent with a SOMO $16a_1$ (Figure 2).

$Ti_2(\mu{:}\eta^5{,}\eta^5\text{-}Pn)_2CO_2$

The CO_2 adduct $Ti_2(\mu{:}\eta^5{,}\eta^5\text{-}Pn^{\dagger})_2CO_2$ has been spectroscopically characterised in solution at low temperature, but is too unstable to be isolated.[17] Optimising the geometry of $Ti_2Pn_2CO_2$ from various

starting geometries led to a minimum energy structure with C_{2v} symmetry, **3**. Selected geometric parameters are given in Table 1.

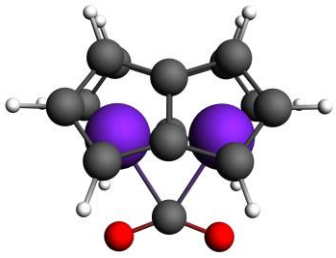

3

The Ti-Ti distance is short (2.41 Å) indicating strong bonding between the Ti atoms. The pentalene rings are bent back slightly more than in Ti_2Pn_2. Examination of the MO of **3** (Figure 8) shows that the key bonding interaction is between the LUMO of bent CO_2 and primarily the HOMO of **2**, ($16a_1$) to form a stabilised orbital, $18a_1$, 2.4 eV more stable than the Ti-Ti bonding orbital. In localised bonding terms the two M-M bonds are replaced by one M-M bond and a 3c-2e bond linking the C of the CO_2 to the M atoms. The two O atoms have a favourable but weak interaction with the Ti atoms accounting for the relatively long Ti-O distance (2.27 Å).

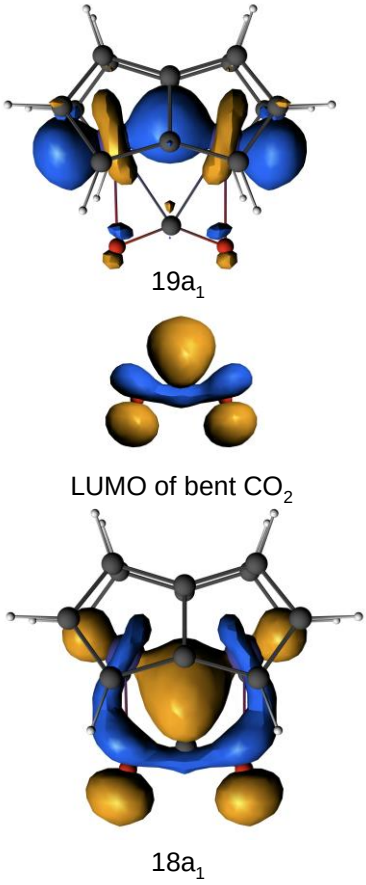

Figure 8. Ti-Ti bonding orbital of $Ti_2Pn_2CO_2$ ($19a_1$), LUMO of bent CO_2 and bonding orbital ($18a_1$) resulting from nucleophilic attack of Ti_2Pn_2 on CO_2.

Further insight into the binding of CO_2 is given by a fragment analysis. On bending, the LUMO of CO_2 is of a_1 symmetry and acts as an acceptor orbital. The CO_2 HOMO and HOMO-1, located on the O atoms, are of a_2 and b_2 symmetry. Thus donation from these into the LUMO of Ti_2Pn_2, which is of a_1 symmetry is forbidden. Fragment analysis enables the energies of bonding interaction of the Ti_2Pn_2 fragment with the CO_2 fragment to be separated according to symmetry. The energies attributable to the various interactions are given in Table 3. The energy values confirm that donation from the HOMO of Ti_2Pn_2 is the predominant bonding interaction. The occupancies of the LUMO, HOMO and HOMO-1 of the Ti_2Pn_2 fragment in **3** are given in Table 4. Some remixing does occur between the HOMO and LUMO but on the whole the HOMO-1 of Ti_2Pn_2 retains its integrity to form the HOMO of the CO_2 derivative, $19a_1$ (Figure 8). Thus CO_2 may be regarded as acting as a μ-Z ligand.

Table 3. Energies (eV) of orbital interactions divided according to their symmetry. The various molecules with C_{2v} symmetry are divided into Ti_2Pn_2 and ligand fragments.

	3	**4**	**7**	**9**	**13**
A_1	-116	-192	-81	-186	-80
A_2	-2	-4	-15	0	-1
B_1	-7	-8	-8	-136	-100
B_2	-15	-21	-24	-165	-125

Table 4. Occupancies of the fragment orbitals of Ti_2Pn_2 in the molecular calculations for **2**, **3**, **4**, **5**, **6**. **7**, **8**, **9** and **13**.

	$14b_2$	**$13b_2$**	**$17a_1$**	**$16a_1$**	**$15a_1$**
2	0	0	0	2.00	2.00
3	0.07	0.09	0.18	0.98	1.99
4	0.22	0.14	0.29	0.77	1.97
5	0.13	0.12	0.23	0.89	1.98
6	0.02	0.07	0.57	1.02	2.00
7	0	0	0.39	1.31	1.97
8	0.33	0.83	0.56	0.70	1.43
9	0.03	0.10	0.12	0.42	1.46
13	0.11	0.25	0.06	0.67	1.97

$Ti_2(\mu:\eta^5,\eta^5\text{-}Pn)_2CS_2$

The adduct of CO_2 to $Ti_2Pn^{\dagger}_2$ has not been structurally characterised but the product of CS_2 addition has.[17] Geometry optimisation of $Ti_2Pn_2CS_2$ led to structure **4,** analogous to **3**. Key structural parameters are given in Table 1 and selected MOs are shown in Figure 9. The Ti-Ti distance is again consistent with significant Ti-Ti bonding. The Ti-C distance is 0.09 Å longer than the CO_2 analogue. The Ti-S distance is 0.27 Å longer than the Ti-O distance whereas the covalent radii differ by 0.39 Å,[35] indicating a more significant interaction for S with Ti than for O. The angles at C are very similar (137° **3**, 138° **4**).

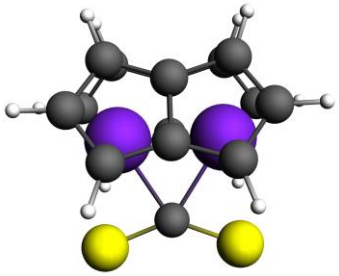

4

On coordination of CS_2, one Ti-Ti bonding orbital, $19a_1$, remains intact, as is the case for the CO_2 complex. The orbital $18a_1$, responsible for CS_2 binding is more delocalised and multicentred than the analogue in **3** consistent with the differences in distance discussed above. Sulfur, with its higher energy orbitals, is having a greater interaction with the Ti atoms. The fragment analysis reinforces this view. Not only is the a_1 interaction energy greater than for **3** (Table 3) but there is also greater Ti_2Pn_2 HOMO LUMO mixing indicating both donor and acceptor quality in the bonding interaction (Table 4). The higher lying orbitals of b_2 symmetry have greater fragment occupancy in **4** than in **3** (Table 4) denoting donation from the b_2 HOMO of bent CS_2. Examination of the overlap population matrices for the two molecules gives a value of 0.19 for **4** significantly greater than the 0.05 for **3**. The calculated charges on O and S in the two molecules also reinforces the view of S being a better donor having a less negative charge (O -0.60, S -0.09 Mulliken; O -0.21, S -0.05 Hirshfeld; O -0.20, S -0.08 Voronoi).

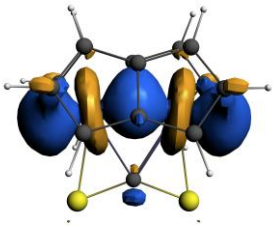

$19a_1$

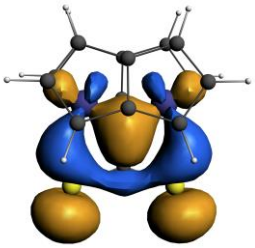

$18a_1$

Figure 9. Ti-Ti bonding orbital, $19a_1$ and Ti_2-CS_2 bonding orbital, $18a_1$ of **4**, $Ti_2Pn_2CS_2$

Ti_2Pn_2COS

The COS adduct, **5**, has been identified in solution but not isolated as it undergoes rapid decomposition below room temperature.[17]

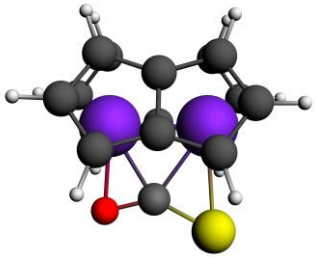

5

The HOMO, $34a_1$, is yet again a Ti-Ti bonding orbital relatively unperturbed on COS binding (Figure 10). The closeness in energy of the Ti_2COS bonding orbital to the $12b_1$ orbital of the Ti_2Pn_2 pentalene unit leads to the two being mixed to form the $33a_1$ and $32a_1$ MO (Figure 10); the lower symmetry caused by COS enables this mixing to take place. The fragment calculation (Table 4) reveals a situation for **5** intermediate between **3** and **4**.

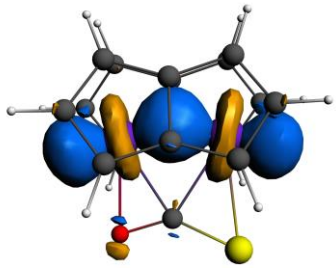

34a'

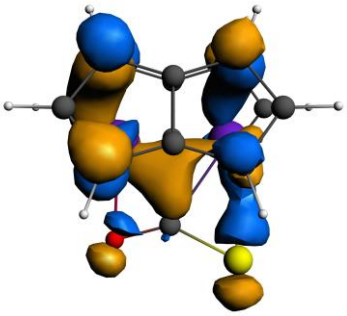

33a'

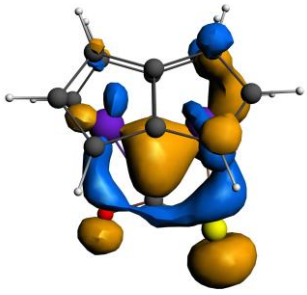

32a'

Figure 10. Top three occupied orbitals of **5**, Ti_2Pn_2COS.

The binding energies of the triatomic ligands to Ti_2Pn_2 are in the order $CS_2 > COS > CO_2$ (Table 5).

Table 5. Calculated SCF binding energies (ΔE) and standard free energies (ΔG^0) in kcal mol^{-1} of ligands to the Ti_2Pn_2 unit.

Compound	Ligands	ΔE	ΔG^0
3	CO_2	-53	-37
4	CS_2	-70	-52
5	COS	-61	-44
6	CO	-48	-31
7	$(CO)_2$	-74	-43
8	$(CO)_3$	-94	-50
12	CO	-19	-5
14	CO	-25	-3

Ti_2Pn_2CO

Given the nature of CO as a π acceptor ligand, symmetric bridging of the two Ti centres by CO is not favoured as the high lying occupied frontier orbitals of Ti_2Pn_2 are of the wrong symmetry. The structure of Ti_2Pn_2CO has C_s symmetry with the CO bound sideways-on to the Ti_2 core, **6**, in agreement with the experimentally determined structure of the monocarbonyl complex $Ti_2(\mu{:}\eta^5,\eta^5\text{-}Pn^{\dagger})_2CO$.[17]

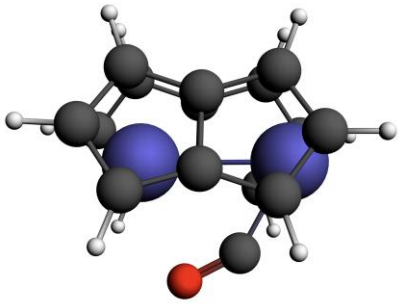

6

Inspection of the orbitals of **6** (Figure 11) indicates that the positioning of CO is steered by back donation from the HOMO of the Ti_2Pn_2 fragment. Once again a Ti-Ti bond is retained forming the HOMO of **6**, 55a. The composition of the two top occupied orbitals in terms of their fragment orbital is given in Table 4. The HOMO-1, 54a, is comprised of one of the 5π orbitals of CO and orbital $16a_1$ of **2**. The calculated wavenumber for the CO stretch is rather lower than the range for symmetric bridging carbonyls, but in good agreement with the experimental value (Table 6).

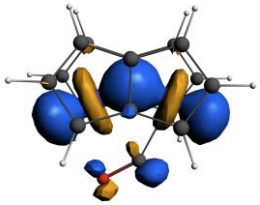

55a

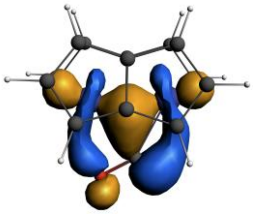

54a

Figure 11. HOMO and HOMO-1 of Ti_2Pn_2CO, **6**.

Table 6. Experimental and calculated (ADF and *Gaussian*) wavenumbers (cm^{-1}) for selected stretching vibrations.

Compound	Mode	Experimental	Calculated
3 $Ti_2Pn_2CO_2$	ν(CO)	Solution: 1678, 1236	1669 (w), 1214 (w) *1601 (w), 1193 (w)*
6 Ti_2Pn_2CO	ν(CO)	Solid: 1655 Solution: not observed	1644 (w) *1532 (w)*
7 $Ti_2Pn_2(CO)_2$	ν(CO)	Solid: 1987 (s), 1910 (m) Solution: 1991 (s), 1910 (w)	1947 (s), 1878 (m) *1899 (s), 1810 (m)*
8 $Ti_2Pn_2(CO)_3$	ν(CO)	Solution: 1991 (w), 1910 (s)	1941 (s), 1894 (s), 1873 (w) *1918 (s), 1868 (s), 1835 (w)*
9 $Ti_2Pn_2O(CO)$	ν(CO)	Not observed	1954 (s) *1942 (s)*
4 $Ti_2Pn_2CS_2$	ν(CS)	Solid: 1101 Solution 1104	1079 (w)
5 Ti_2Pn_2COS	ν(CO)	Solution: 1498	1487 (w) *1428 (w)*
14 $Ti_2Pn_2S(CO)$	ν(CO)	Solution: 2011	1937 (m) *1924 (m)*

$Ti_2Pn_2(CO)_2$

Geometry optimisation of the dicarbonyl adduct $Ti_2Pn_2(CO)_2$ by both computational methods gave a structure of C_s symmetry only slightly displaced from C_{2v} symmetry, **7**. The calculated structure from ADF had an imaginary frequency of a' symmetry with a wavenumber of $-i15$ cm^{-1}. The calculated geometry agrees well with that found experimentally.[16]

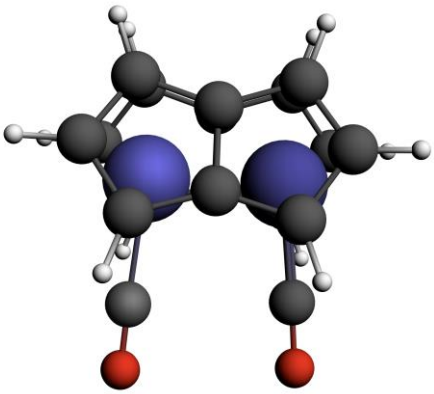

7

The Ti-Ti bonding orbital, 36a (Figure 12) remains intact, consistent with the short Ti-Ti distance of 2.42 Å, but is straighter than found for the other derivatives. Back-bonding to both CO groups occurs in orbital 35a, which has clear origins in the $6b_{3u}$ orbital of **1**.

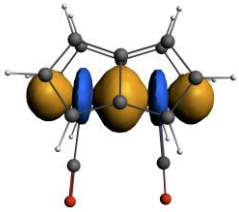

36a

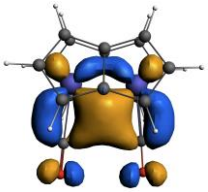

35a

Figure 12. HOMO and HOMO-1 of **7**, $Ti_2Pn_2(CO)_2$.

Agreement between the experimental and calculated stretching wavenumbers (Table 6) follows the same pattern as for the monocarbonyl, **6.** Although binding of CO to the monocarbonyl **6** is energetically favourable, the ligand redistribution of **6** to afford **7** and **2** in the absence of CO is not predicted to be spontaneous (Table 5).

$Ti_2Pn^{\dagger}_2(CO)_3$

It was previously observed that reaction of $Ti_2Pn^{\dagger}_2$ with excess CO at -78 °C produced an orange-brown solution, which following removal of the reaction headspace *in vacuo* and warming to room temperature resulted in a colour change to green-brown, characteristic of the dicarbonyl complex $Ti_2Pn^{\dagger}_2(CO)_2$.[16] These observations hinted that an additional product is formed in the presence of excess CO at low temperatures, which was investigated by variable temperature NMR spectroscopy. A solution of $Ti_2Pn^{\dagger}_2(^{13}CO)_2$ in methylcyclohexane-d_{14} was sealed under ^{13}CO and the $^{13}C\{^1H\}$ NMR spectrum at 30 °C (Figure 13) showed a very broad resonance centred at 232 ppm ($\Delta\nu_{½}$ = 190 Hz). The spectrum was resolved by cooling to -70 °C (Figure 13), with two peaks in *ca.* 2:1 ratio at 268 and 257 ppm assigned to two chemically inequivalent carbonyl environments in $Ti_2Pn^{\dagger}_2(^{13}CO)_3$, and a peak at 186 ppm corresponding to free ^{13}CO in solution. These three ^{13}C peaks broaden upon warming and coalesce at 0 °C (Figure 13), consistent with a dynamic intermolecular exchange process with free ^{13}CO. A ^{13}C-^{13}C EXSY experiment at -40 °C (mixing time = 500 ms) showed cross-peaks between the bridging and terminal carbonyl signals which implies there is also an exchange process occurring between these CO sites in $Ti_2Pn^{\dagger}_2(CO)_3$ (Scheme 1).

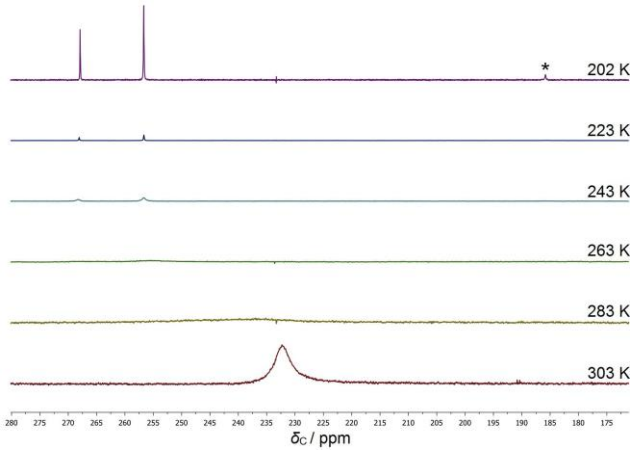

Figure 13. Selected VT $^{13}C\{^1H\}$ NMR spectra of $Ti_2Pn^{\dagger}_2(^{13}CO)_3$ in MeCy-d_{14} solution (the temperature increases down the page in 20 K increments). Asterisk indicates free CO.

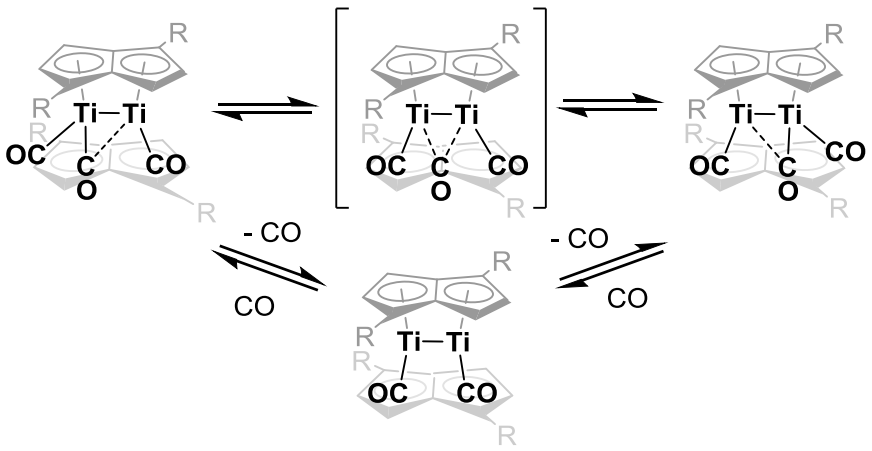

Scheme 1. Reactivity of $Ti_2Pn^{\dagger}_2(CO)_2$ with CO. R = Si^iPr_3.

The carbonylation of $Ti_2Pn^{\dagger}_2$ in methylcyclohexane solution at -55 °C was studied by *in situ* IR spectroscopy, showing initial growth of an IR band at 1992 cm^{-1} which then decreases in intensity and levels off as a *ν*(CO) stretch at 1910 cm^{-1} grows in (Figure 14). This lower energy *ν*(CO) stretch became the major IR band at -55 °C once gas addition was complete. At 26 °C under CO the intensities of the two bands reversed, with 1992 cm^{-1} as the major *ν*(CO) stretching band. Removal of the CO headspace *in vacuo* led to near complete removal in the lower energy *ν*(CO) stretch at 1910 cm^{-1} (see SI Figure S9). These results suggest that the band centred at 1992 cm^{-1} is $Ti_2Pn^{\dagger}_2(CO)_2$, which is the major product in the initial stages of reaction and upon warming to 26 °C when CO becomes less soluble. The IR band at 1910 cm^{-1} is assigned to the terminal *ν*(CO) stretch in $Ti_2Pn^{\dagger}_2(CO)_3$, which is the major product in solution under excess CO at -55 °C, but diminishes upon exposure to vacuum and warming to room temperature. An analogous experiment was performed using ^{13}CO, and gave similar qualitative results with IR bands at 1948 cm^{-1} and 1867 cm^{-1} assigned to the terminal *ν*(CO) in $Ti_2Pn^{\dagger}_2(^{13}CO)_2$ and $Ti_2Pn^{\dagger}_2(^{13}CO)_3$ respectively. IR bands for the bridging CO ligands, expected in the region 1850-1600 cm^{-1},[36] were not observed in the solution spectra for $Ti_2Pn^{\dagger}_2(CO)$ and $Ti_2Pn^{\dagger}_2(CO)_3$, possibly due to extensive broadening.

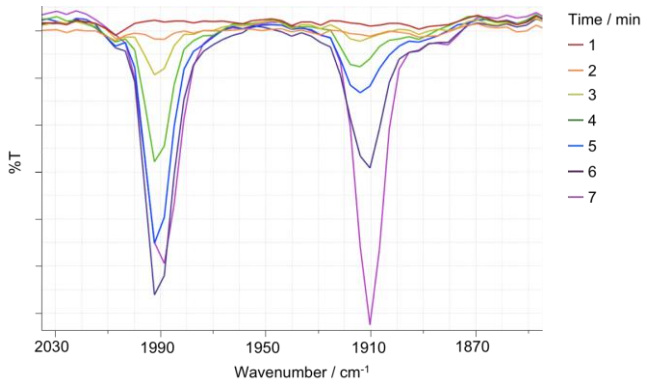

Figure 14. *ν*(CO) region of the React IR spectrum of $Ti_2Pn^{\dagger}_2$ with CO at -55 °C.

Orange crystals of $Ti_2Pn^{\dagger}_2(CO)_3$ were grown under an atmosphere of CO from a saturated toluene solution stored at -80 °C. Unfortunately analysis by single crystal X-ray diffraction was hampered by their deterioration when placed in oil for mounting, with effervescence of gas accompanying decomposition of the crystals. However, elemental analysis of the orange crystals was consistent with the proposed formulation of $Ti_2Pn^{\dagger}_2(CO)_3$.

$Ti_2Pn_2(CO)_3$

Experimental evidence for a tricarbonyl species prompted the search for a computational analogue, $Ti_2Pn_2(CO)_3$, which optimised to structure **8**.

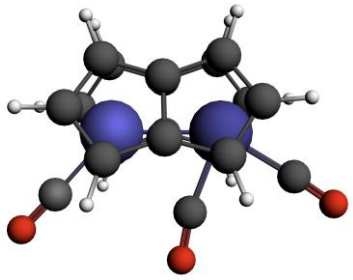

8

The Ti-Ti distance in **8** is significantly longer than in found in structures **1**-**7**. The structure is asymmetric with two terminal carbonyls and one semi-bridging. The two highest occupied orbitals, 55a and 54a, (Figure 15) are principally involved in back-donation to the CO ligands. The HOMO 55a is focused on the Ti with just one bound CO contributing a π* orbital. MO 54a binds the other two CO ligands but retains a small amount of Ti-Ti bonding character.

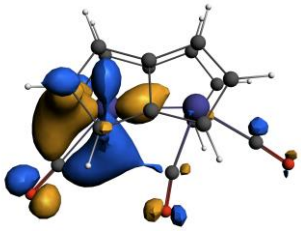

65a

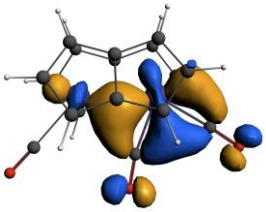

64a

Figure 15. Ti-CO backbonding orbitals of $Ti_2Pn_2(CO)_3$, **8**.

The Ti_2Pn_2 fragment occupations are in accord with the reduction in metal-metal bonding (Table 4). The occupancy of the $15a_1$ Ti-Ti bonding orbital is reduced compared to the examples above showing that in the case of **8** both Ti-Ti bonding orbitals of Ti_2Pn_2 are involved in back donation. In addition occupancy of the LUMO+1 and the LUMO+2 ($13b_2$ and $14b_2$) is significant and these have Ti-Ti anti-bonding character. The calculated CO stretching wavenumbers (Table 6) suggest that one of the three expected vibrations is coincident with the higher stretching frequency of the dicarbonyl. The second one, of lower energy, is stronger than the lower stretch of the dicarbonyl and that the third is too weak to be observed. These predictions fit well with the dynamic behavior of $Ti_2Pn^{\dagger}_2(CO)_3$ in the spectroscopic studies described above.

If $Ti_2Pn^{\dagger}_2(CO)_3$ also has three inequivalent carbonyls as suggested by the computed structure **8**, three ^{13}CO signals are expected in the low temperature NMR. As reported above, at -70 °C (Figure 13) only two are observed. The obvious inference is that the two outer CO groups are rendered chemically equivalent on the NMR timescale by means of the inner CO oscillating between them, in what might be described as a 'ping-pong' mechanism (see Scheme 1). It is proposed that the exchange between bridging and terminal CO sites occurs indirectly via an intermolecular process.

Ti_2Pn_2O

Decomposition of $Ti_2Pn^{\dagger}_2CO_2$ proceeds via a mono(oxo) product, which can be synthesised independently by action of N_2O on $Ti_2Pn^{\dagger}_2$.[17] Maintenance of the sandwich structure of the Ti_2Pn_2

fragment leads to a local minimum with C_{2v} symmetry, structure **9**. With η^8-coordination of Pn to Ti two other structures were found, one with a triplet state, **10**, and the other with a singlet state, **11**.

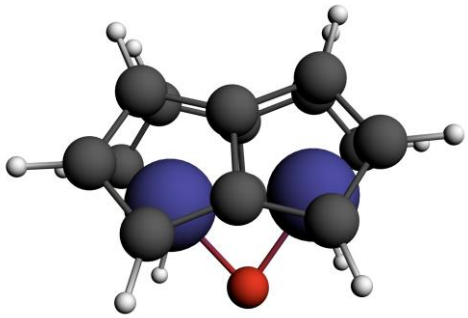

9

The structures found for the triplet state by the two methods differed in the Ti-O-Ti angle. ADF calculations optimised to a bent angle while the Gaussian calculations gave a linear Ti-O-Ti unit. Similar structures were found for the singlet state with η^8-coordination by the two computational methods (Table 1).

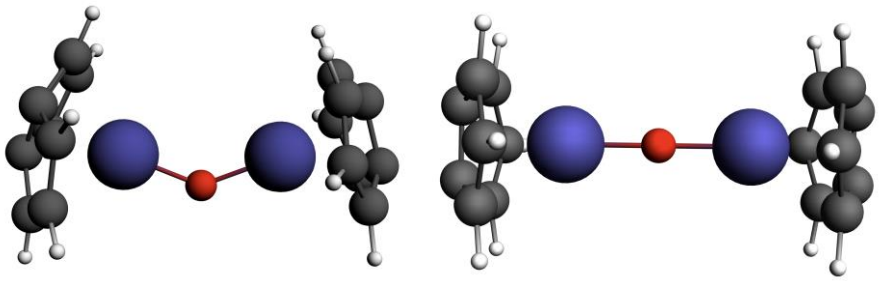

10(ADF) **10(Gaussian)**

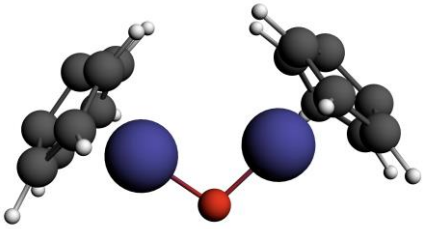

11

The energies of all three structures are close and the most stable is method and temperature dependent (Table 7). ADF(BP/TZP) has the sandwich structure the most stable. Gaussian(B3LYP/SDD) estimates the SCF energy of the sandwich structure to be the lowest but the free energy at 298 K gives the triplet

η^8-coordinated structure to be the most stable. This in agreement with experiment as the sandwich structure is known to convert to the triplet state at room temperature.[17]

Table 7. Relative energies (kcal mol^{-1}) of structures found for Ti_2Pn_2O.

	ΔE(SCF)	ΔH^0_{298}	ΔG^0_{298}
10	0, *0*	0, *0*	0, *2*
11	12, *4*	13, *3*	8, *0*
12	12, *19*	13, *21*	10, *20*

Structure **9** has a Ti-Ti bonding orbital, $17a_1$ (Figure 16). The high symmetry of the molecule facilitates identification of orbitals associated with Ti-O bonding, $14a_1$ and $12b_2$. All three 2p orbitals of O contribute to its bonding as illustrated by the binding energies decomposed by the symmetry of the orbitals involved (Table 3). The O atom competes effectively with the pentalene ligands for the Ti 3d orbitals as evidenced by the increased Ti ring centroid distances (Table 1).

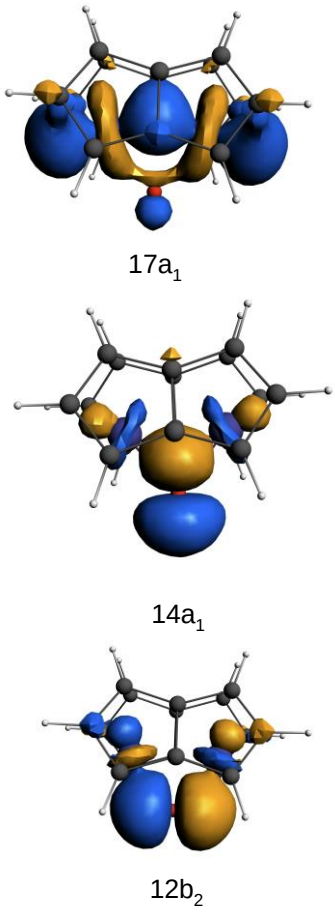

Figure 16. Ti-Ti and Ti-O bonding orbitals of Ti_2Pn_2O, **9**.

Orbitals containing the metal based electrons of **10**(ADF) and **11** are shown in Figure 17. Orbital 53a of **11** shows a bent Ti-Ti bond, the cause of the more acute angle at O in **11** (Table 1).

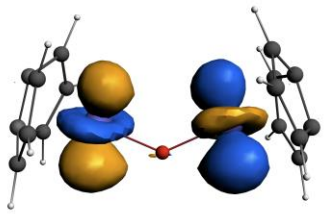

10 54a α

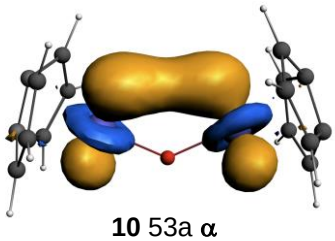

10 53a α

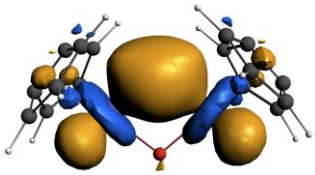

11 53a

Figure 17. Metal based orbitals of PnTiOTiPn in both triplet, **10**, and singlet, **11**, states.

$Ti_2Pn_2(\mu\text{-}O)(CO)$

A possible intermediate in the decomposition of $Ti_2Pn_2CO_2$, undetected as yet experimentally, is $Ti_2Pn_2(\mu\text{-}O)CO$ in which a CO bond has broken, the detached O bridges the two Ti atoms and the CO ligand formed is bonded to one of the Ti atoms. Geometry optimisation gave a local minimum for such a species, **12**. The Ti-Ti distance (2.46, *2.43* Å) is still indicative of Ti-Ti bonding but longer than found for **9**. The bridging O is placed asymmetrically, further from the Ti that also has the CO coordinated.

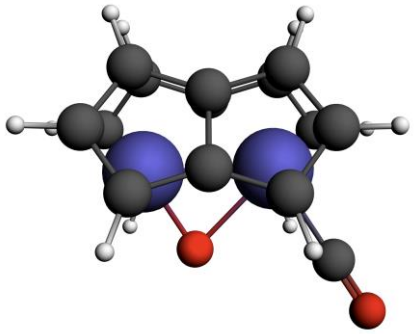

12

The HOMO of **12** (Figure 18) forms a Ti-Ti bond but also has a role in back-bonding to the CO. The CO stretching vibration has a high wavenumber (1954, *1945* cm^{-1}) consistent with the small amount of back-bonding indicated by the HOMO. Binding of the bridging oxo ligand is spread over several MOs and is both σ and π in character. The O π-bonding competes with the pentalene binding and results in an increase in Ti-Pn ring C distances (Table 1).

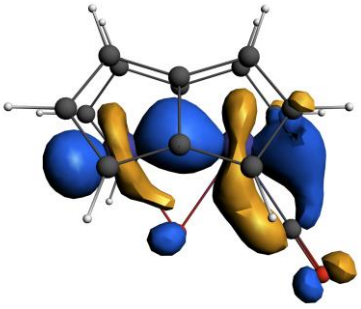

Figure 18. HOMO of $Ti_2Pn_2O(CO)$, **12**.

The energies of **3** and 1**2** are very close; ADF calculates **12** to be 1 kcal mol^{-1} less stable than **3** whereas Gaussian predicts **12** to be 11 kcal mol^{-1} more stable than **3**.

Ti_2Pn_2S

The mono-sulfide derivative $Ti_2Pn^{\dagger}{}_2S$ can be synthesised by reaction of $Ti_2Pn^{\dagger}{}_2$ with Ph_3PS.[17] Geometry optimisation of Ti_2Pn_2S, **13**, gave a structure with dimensions in good agreement with the X-ray structure of $Ti_2Pn^{\dagger}{}_2S$.[17]

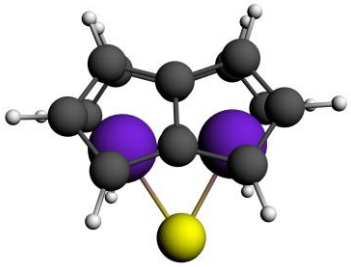

13

The Ti-Ti distance in **13** is longer than that calculated for the oxo analogue **9** but indicates Ti-Ti bonding. The HOMO of **13,** $13b_1$, is largely localised on the S and lies close in energy to the Ti-Ti bonding orbital $17a_1$ (Figure 19). Separation of the bonding interactions by symmetry shows a different pattern from the oxo analogue in that the b_2 interaction is the strongest and the a_1 interaction the weakest although all three S 3p orbitals contribute significantly to the bonding (Table 3). The Ti_2Pn_2 fragment occupancies (Table 4) also indicate less donation from the Ti atoms to the S than is found for O.

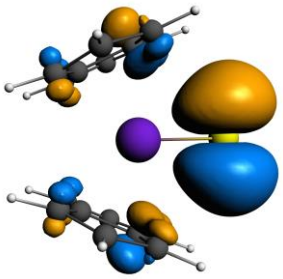

$13b_1$

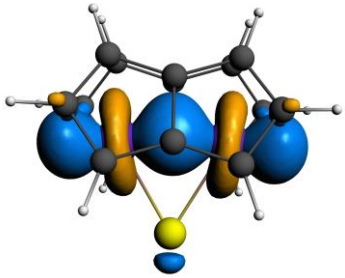

$17a_1$

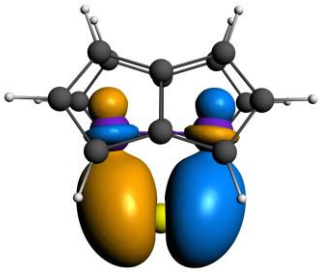

$12b_2$

Figure 19. Selected orbitals for Ti_2Pn_2S, **13.**

$Ti_2Pn_2S(CO)$

There is good NMR evidence that $Ti_2Pn^{\dagger}{}_2S$ binds CO reversibly.[17] Geometry optimisation of $Ti_2Pn_2S(CO)$, **14**, gives a similar structure to **12**.

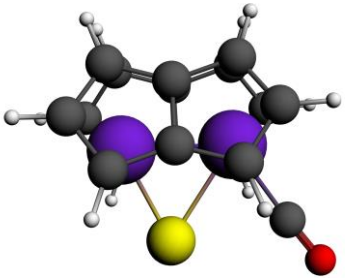

14

Binding of CO utilises the Ti-Ti bonding orbital of **13** as found for **12** as shown in Figure 20.

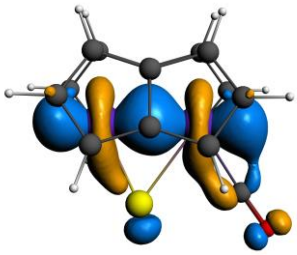

Figure 20. Isosurface of the 34a' orbital of **14** showing back donation to CO from the Ti-Ti bonding orbital.

The Ti-Ti distance calculated for **14** is slightly longer than for **12** (Table 1) and the calculated CO stretch slightly lower (Table 6), both comparisons suggesting that donation from the Ti-Ti bonding orbital is greater for **14**, consistent with the lower electronegativity of S compared with O. The CO

ligand has a rather low free energy of binding (Table 5) consistent with rapid exchange in solution as evidenced by the NMR spectrum.[17]

The relative energies calculated for **14** and **5** differ from the oxo analogues; both methods predict **14** to be more stable (ADF(BP/TZP) by 14 kcal mol^{-1}, Gaussian(B3LYP/SDD) by 9 kcal mol^{-1}).

$PnTi(O)_2TiPn$

$Pn^{\dagger}Ti(\mu\text{-}O)_2TiPn^{\dagger}$ is one of the products obtained from the reductive disproportionation of CO_2 by $Ti_2Pn^{\dagger}_2$, and structural parameters of the optimised structure of $PnTi(\mu\text{-}O)_2TiPn$, **15**, (Table 1) are in good agreement with those obtained experimentally.[17] There is no Ti-Ti bonding the Ti atoms being in the IV oxidation state, the Ti-Ti distance of 2.74 Å (Table 1) is constrained by the short bonds to the bridging O atoms.

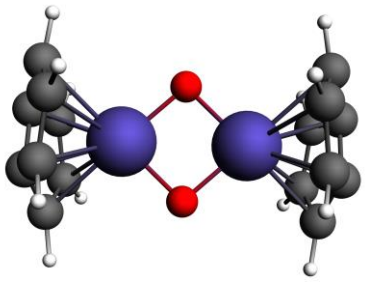

15

The HOMO and HOMO-1 (Figure 21) represent δ bonds binding the pentalene ligands.

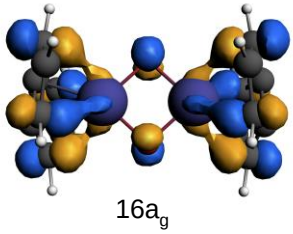

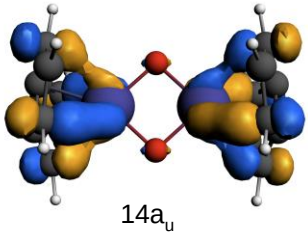

Figure 21. HOMO and HOMO-1 of $PnTiO_2TiPn$.

CONCLUSIONS

Ti_2Pn_2 has three frontier orbitals, two occupied high lying metal-metal bonding orbitals and one low lying LUMO, which enable this particular complex to display a range of reactivity not found with other double sandwich compounds of this class. Its electron rich nature dominates the chemistry and it acts as a donor to CO_2, CS_2 and COS and is able to bind one, two and three CO groups. The three frontier orbitals are of a_1 symmetry and as a consequence a single CO molecule binds in a sideways manner. Complexes may be formed with O and S, which maintain the sandwich structure and in these cases the chalcogen atoms compete effectively with the pentalene ligands for the Ti d orbitals and form strong interactions of a_1, b_1 and b_2 symmetry involving all three chalcogen p orbitals. All compounds which maintain the double sandwich structure of Ti_2Pn_2 have a Ti-Ti single bond.

EXPERIMENTAL SECTION

Computational methods

Density functional calculations were carried out using two methods. One employed the Amsterdam Density Functional package (version ADF2012.01).[37] The Slater-type orbital (STO) basis sets were of triple-ζ quality augmented with a one polarization function (ADF basis TZP). Core electrons were frozen (C 1s; Ti 2p) in our model of the electronic configuration for each atom. The local density approximation (LDA) by Vosko, Wilk and Nusair (VWN)[38] was used together with the exchange correlation corrections of Becke and Perdew (BP86).[39-41] The other used Gaussian (version 09 revision A.02)[42] with the B3LYP functional and SDD basis sets. In both sets of calculations tight optimisation conditions were used and frequency calculations were used to confirm stationary points. Using the ADF code, molecules were subjected to fragment analyses where the MOs of fragments, with the same geometry as they possess in the molecules, were used as the basis set for a full molecular calculation.

General synthetic procedures

All manipulations were carried out using standard Schlenk techniques under Ar, or in an MBraun glovebox under N_2 or Ar. All glassware was dried at 160 °C overnight prior to use. Solvents were purified by pre-drying over sodium wire and then distilled over Na (toluene), K (methylcyclohexane) or Na-K alloy (Et_2O, hexane and pentane) under a N_2 atmosphere. Dried solvents were collected, degassed and stored over argon in K mirrored ampoules. Deuterated solvents were degassed by three freeze−pump−thaw cycles, dried by refluxing over K for 3 days, vacuum distilled into ampoules and

stored under N_2. The gases used were of very high purity - CO (99.999%) and isotopically enriched ^{13}CO (99.7%) were supplied by Union Carbide and Euriso-top respectively, and were added *via* Toepler pump. The compound $Ti_2Pn^{\dagger}_2$ was prepared according to published procedures.[14] NMR spectra were recorded on a Varian VNMRS 400 (^1H 399.5 MHz; $^{13}C\{^1H\}$ 100.25 MHz; $^{29}Si\{^1H\}$ 79.4 MHz) spectrometer. The spectra were referenced internally to the residual protic solvent (^1H) or the signals of the solvent (^{13}C). $^{29}Si\{^1H\}$ NMR spectra were referenced externally relative to $SiMe_4$. IR spectra were recorded between NaCl plates using a Perkin-Elmer Spectrum One FTIR instrument or using a Mettler-Toledo ReactIR system featuring an IR probe inside a gas tight cell attached to a Toepler pump. CW-EPR spectroscopy was carried out by Dr W. K. Meyers from the CÆSR Facility at the University of Oxford using an X-band Bruker EMXmicro spectrometer. Simulations were made with the Win-EPR suite. Mass spectra were recorded using a VG Autospec Fisons instrument (EI at 70 eV). Elemental analyses were carried out by S. Boyer at the Elemental Analysis Service, London Metropolitan University. Solid state magnetic measurements were carried out by A.-C. Schmidt at FAU Erlangen, using a Quantum Design MPMS-5 SQUID magnetometer. Accurately weighed samples (*ca.* 20 mg) were placed into gelatine capsules and then loaded into nonmagnetic plastic straws before being lowered into the cryostat. Samples used for magnetisation measurements were recrystallised multiple times and checked for chemical composition and purity by elemental analysis and EPR spectroscopy. Values of the magnetic susceptibility were corrected for the underlying diamagnetic increment by using tabulated Pascal constants,[43] and the effect of the blank sample holders (gelatin capsule/straw).

Synthesis of $[Ti_2(\mu{:}\eta^5,\eta^5\text{-}Pn^{\dagger})_2][B(C_6F_5)_4]$

To a stirred, solid mixture of $Ti_2Pn^{\dagger}_2$ (132 mg, 0.143 mmol) and $[FeCp^*_2][B(C_6F_5)_4]$ (143 mg, 0.142 mmol) at -35 °C was added Et_2O (20 mL), pre-cooled to -78 °C, and the resultant brown mixture was allowed to warm to room temperature. After 12 h the solvent was removed under reduced pressure to afford a brown residue that was washed thoroughly with pentane (4 × 20 mL) to remove $FeCp^*_2$ until the washings ran colourless. The residue was then extracted with Et_2O (2 × 10 mL), concentrated to *ca.* 5 mL and 5 drops of hexane were added. Cooling this solution to -35 °C produced brown-green crystals, which were isolated by decantation and dried *in vacuo*. Total yield: 125 mg (55% with respect to $Ti_2Pn^{\dagger}_2$). ^{19}F NMR (THF-d_8, 375.9 MHz, 303 K): δ_F -132.7 (br, *o-F*), -165.2 (t, $^3J_{FF}$ = 20.2 Hz, *p-F*), -168.7 (br t, $^3J_{FF}$ = 19.3 Hz, *m-F*). $^{11}B\{^1H\}$ NMR (THF-d_8, 128.2 MHz, 303 K): δ_B -14.75. EPR (solid state, 293 K, X-band): g_1 = 2.003, $g_2 = g_3$ = 1.944, g_{iso} = 1.964. EI-MS: No volatility. Anal. found (calcd. for $C_{76}H_{92}BF_{20}Si_4Ti_2$): C, 56.72 (56.89); H, 5.83 (5.78) %. Mag. suscep. (Evans method, THF-d_8, 303 K): μ_{eff} = 1.96 μ_B per dimer; (SQUID, 260 K): μ_{eff} = 1.92 μ_B per dimer. Crystal data for

$[B(C_6F_5)_4].½(C_6H_{14})$: $C_{79}H_{99}BF_{20}Si_4Ti_2$, M_r = 1647.55, triclinic, space group *P-1*, green plate, a = 14.217(3) Å, b = 15.491(3) Å, c = 19.366(4) Å, α = 89.30(3)°, β = 88.71(3)°, γ = 67.67(3)°, V = 3944.1(16) Å^3, T = 100 K, Z = 2, R_{int} = 0.079, $\lambda_{Mo}(K\alpha)$ = 0.71075 Å, θ_{max} = 26.372°, R_1 [$I > 2\sigma(I)$] = 0.0562, wR_2 (all data) = 0.1656, *GooF* = 1.025.

Synthesis of $(\mu{:}\eta^5,\eta^5\text{-}Pn^\dagger)_2Ti_2(CO)_3$

To a degassed solution of $Ti_2Pn^\dagger_2(CO)_2$ (10 mg, 0.0108 mmol) in methylcyclohexane-d_{14} (0.5 mL) at -78 °C was added ^{13}CO (0.85 bar). Warming of the mixture resulted in a colour change from green-brown to orange-brown. NMR yield: quantitative with respect to $Ti_2Pn^\dagger_2(CO)_2$. ^1H NMR (methylcyclohexane-d_{14}, 399.5 MHz, 303 K): δ_H 7.31 (2H, d, $^3J_{HH}$ = 2.9 Hz, Pn *H*), 7.22 (2H, br s, $\Delta\nu_{½}$ = 10 Hz, Pn *H*), 5.10 (2H, d, $^3J_{HH}$ = 2.8 Hz, Pn *H*), 4.96 (2H, d, $^3J_{HH}$ = 3.0 Hz, Pn *H*), 1.59 (6H, m, ^{i}Pr C*H*), 1.43 (6H, m, ^{i}Pr C*H*), 1.20 (18H, d, $^3J_{HH}$ = 7.4 Hz, ^{i}Pr CH_3), 1.17 (18H, d, $^3J_{HH}$ = 7.4 Hz, ^{i}Pr CH_3), 1.08 (18H, d, $^3J_{HH}$ = 7.4 Hz, ^{i}Pr CH_3), 0.93 (18H, d, $^3J_{HH}$ = 7.4 Hz, ^{i}Pr CH_3). ^1H NMR (methylcyclohexane-d_{14}, 399.5 MHz, 193 K): δ_H 7.00 (2H, s, Pn *H)*, 6.00 (2H, s, Pn *H*), 5.47 (2H, s, Pn *H*), 5.29 (2H, s, Pn *H*), 1.60 (6H, s, ^{i}Pr C*H*), 1.44 (6H, s, ^{i}Pr C*H*), 1.26 - 1.08 (36H, overlapping m, ^{i}Pr CH_3), 1.02 (18H, s, ^{i}Pr CH_3), 0.84 (18H, s, ^{i}Pr CH_3). $^{13}C\{^1H\}$ NMR (methylcyclohexane-d_{14}, 100.5 MHz, 303 K): δ_C 232.1 (br, $\Delta\nu_{½}$ = 190 Hz, *C*O), 128.3 (Pn *C*), 123.3 (Pn *C*), 123.0 (Pn *C*), 122.8 (Pn *C*), 106.3 (Pn *C*), 103.9 (Pn *C*), 91.3 (Pn *C*), 86.2 (Pn *C*), 21.0 (^{i}Pr *C*H$_3$), 20.9 (^{i}Pr *C*H$_3$), 20.8 (^{i}Pr *C*H$_3$), 20.4 (^{i}Pr *C*H$_3$), 15.3 (^{i}Pr *C*H), 13.9 (^{i}Pr *C*H). $^{13}C\{^1H\}$ NMR (methylcyclohexane-d_{14}, 100.5 MHz, 193 K): δ_C 267.8 (*C*O), 256.7 (*C*O), 185.9 (free *C*O), 128.6 (Pn *C*), 119.0 (Pn *C*), 115.1 (Pn *C*), 114.5 (Pn *C*), 100.3 (Pn *C*), 96.2 (Pn *C*), 91.6 (Pn *C*), 90.5 (Pn *C*), 21.2 (^{i}Pr *C*H$_3$), 21.0 (^{i}Pr *C*H$_3$), 20.9 (^{i}Pr *C*H$_3$), 15.4 (^{i}Pr *C*H), 13.5 (^{i}Pr *C*H). $^{29}Si\{^1H\}$ NMR (methylcyclohexane-d_{14}, 79.4 MHz, 303 K): δ_{Si} 3.59, 3.09. IR (methylcyclohexane, -65 °C): $Ti_2Pn^\dagger_2(^{12}CO)_2$ 1991 (w, νCO), 1910 (s, νCO); $Ti_2Pn^\dagger_2(^{13}CO)_2$ 1948 (w, ν^{13}CO), 1867 (s, ν^{13}CO) cm^{-1}. EI-MS: *m/z* = 923 (100%), [M - 3CO]$^+$. Anal. found (calcd. for $C_{55}H_{92}O_3Si_4Ti_2$): C, 65.53 (65.44); H, 9.27 (9.19) %.

Crystallographic Details

Single crystal XRD data for $[Ti_2(\mu{:}\eta^5,\eta^5\text{-}Pn^\dagger)_2][B(C_6F_5)_4]$ were collected by the UK National Crystallography Service (NCS),[44] at the University of Southampton on a Rigaku FR-E+ Ultra High Flux diffractometer ($\lambda_{Mo\ K\alpha}$) equipped with VariMax VHF optics and a Saturn 724+ CCD area detector. The data were collected at 150 K using an Oxford Cryosystems Cobra low temperature device. Data collected by the NCS were processed using CrystalClear-SM Expert 3.1 b18,[45] and unit cell parameters

were refined against all data. Data were processed using CrysAlisPro (version 1.171.36.32),[46] and unit cell parameters were refined against all data. An empirical absorption correction was carried out using the Multi-Scan program.[47] The structure was solved using SHELXL-2013,[48] and refined on F_o^2 by full-matrix least-squares refinements using SHELXL-2013.[48] Solutions and refinements were performed using the OLEX2[49] or WinGX[50] packages and software packages within. All non-hydrogen atoms were refined with anisotropic displacement parameters. All hydrogen atoms were refined using a riding model.

ASSOCIATED CONTENT

Supporting Information. Detailed X-ray, IR, EPR, NMR and CV data; a text file of computed molecule Cartesian coordinates for all structures in .xyz format for convenient visualization; crystallographic data for $[Ti_2(\mu{:}\eta^5,\eta^5\text{-}Pn^{\dagger})_2][B(C_6F_5)_4]$ in CIF format. This material is available free of charge via the Internet at http://pubs.acs.org.

AUTHOR INFORMATION

Email for FGNC: f.g.cloke@sussex.ac.uk. Email for JCG: jennifer.green@chem.ox.ac.uk.

The authors declare no competing financial interests.

ACKNOWLEDGEMENTS

We thank the European Research Council and the University of Sussex for financial support. A.-C. Schmidt (SQUID magnetometry), Dr W. K. Meyers (EPR spectroscopy), Dr I. J. Day (NMR spectroscopy) and Dr P. N. Horton (X-ray crystallography) are also acknowledged.

REFERENCES

(1) Summerscales, O. T.; Cloke, F. G. N. *Coord. Chem. Rev.* **2006**, *250*, 1122–1140.
(2) Green, M. *J. Organomet. Chem.* **1995**, *500*, 127–148.
(3) Parkin, G. In *Comprehensive Organometallic Chemistry III*; Crabtree, R. H.; Mingos, D. M. P., Eds.; Elsevier: Oxford, 2006; Vol. 1, pp. 1–57.
(4) *www.covalentbondclass.org*.
(5) Cloke, F. G. N.; Green, J. C.; Jardine, C. N. *Organometallics* **1999**, *18*, 1087–1090.
(6) Cloke, F. G. N.; Green, J. C.; Kaltsoyannis, N. *Organometallics* **2004**, *23*, 832–835.
(7) Balazs, G.; Cloke, F. G. N.; Gagliardi, L.; Green, J. C.; Harrison, A.; Hitchcock, P. B.; Shahi, A. R. M.; Summerscales, O. T. *Organometallics* **2008**, *27*, 2013–2020.

(8) Katz, T. J.; Acton, N. *J. Am. Chem. Soc.* **1972**, *94*, 3281–3283.
(9) Katz, T. J.; Acton, N.; McGinnis, J. *J. Am. Chem. Soc.* **1972**, *94*, 6205–6206.
(10) Kuchta, M.; Cloke, F. G. N. *Organometallics* **1998**, *17*, 1934–1936.
(11) Balazs, G.; Cloke, F. G. N.; Harrison, A.; Hitchcock, P. B.; Green, J.; Summerscales, O. T. *Chem. Commun.* **2007**, 873–875.
(12) Ashley, A. E.; Cooper, R. T.; Wildgoose, G. G.; Green, J. C.; O'Hare, D. *J. Am. Chem. Soc.* **2008**, *130*, 15662–15677.
(13) Summerscales, O. T.; Rivers, C. J.; Taylor, M. J.; Hitchcock, P. B.; Green, J. C.; Cloke, F. G. N. *Organometallics* **2012**, *31*, 8613–8617.
(14) Kilpatrick, A. F. R.; Green, J. C.; Cloke, F. G. N.; Tsoureas, N. *Chem. Commun.* **2013**, 9434–9436.
(15) Green, J. C.; Green, M. L. H.; Parkin, G. *Chem. Commun.* **2012**, *48*, 11481–11503.
(16) Kilpatrick, A. F. R.; Cloke, F. G. N. *Chem. Commun.* **2014**, *50*, 2769–2771.
(17) Kilpatrick, A. F. R.; Green, J. C.; Cloke, F. G. N. *Manuscript submitted*.
(18) Bendjaballah, S.; Kahlal, S.; Costuas, K.; Bévillon, E.; Saillard, J.-Y. *Chem.–Eur. J.* **2006**, *12*, 2048–2065.
(19) Lauher, J. W.; Hoffmann, R. *J. Am. Chem. Soc.* **1976**, *98*, 1729–1742.
(20) Brintzinger, H. H.; Bartell, L. S. *J. Am. Chem. Soc.* **1970**, *92*, 1105–1107.
(21) Brintzinger, H. H.; Lohr, L. L.; Wong, K. L. T. *J. Am. Chem. Soc.* **1975**, *97*, 5146–5155.
(22) Petersen, J. L.; Dahl, L. F. *J. Am. Chem. Soc.* **1975**, *97*, 6416-6422.
(23) Fieselmann, B. F.; Hendrickson, D. N.; Stucky, G. D. *Inorg. Chem.* **1978**, *17*, 2078–2084.
(24) Albright, T. A.; Burdett, J. K.; Whangbo, M.-H. *Orbital Interactions in Chemistry*; 2nd ed.; John Wiley & Sons, 2013.
(25) Green, J. C. *Chem. Soc. Rev.* **1998**, *27*, 263-271.
(26) Compton, R. G.; Banks, C. E. *Understanding Voltammetry*; 2nd ed.; Imperial College Press, 2011.
(27) Hanna, T. E.; Lobkovsky, E.; Chirik, P. J. *Organometallics* **2009**, *28*, 4079–4088.
(28) Gericke, H. J.; Barnard, N. I.; Erasmus, E.; Swarts, J. C.; Cook, M. J.; Aquino, M. A. S. *Inorg. Chim. Acta* **2010**, *363*, 2222–2232.
(29) Geiger, W. E.; Barrière, F. *Acc. Chem. Res.* **2010**, *43*, 1030–1039.
(30) Bouwkamp, M. W.; de Wolf, J.; Del Hierro Morales, I.; Gercama, J.; Meetsma, A.; Troyanov, S. I.; Hessen, B.; Teuben, J. H. *J. Am. Chem. Soc.* **2002**, *124*, 12956–12957.
(31) Hitchcock, P. B.; Kerton, F. M.; Lawless, G. A. *J. Am. Chem. Soc.* **1998**, *120*, 10264–10265.
(32) Horáček, M.; Kupfer, V.; Thewalt, U.; Štěpnička, P.; Polášek, M.; Mach, K. *Organometallics* **1999**, *18*, 3572–3578.
(33) Evans, J. *J. Chem. Soc.* **1959**, 2003–2005.
(34) Schubert, E. M. *J. Chem. Educ.* **1992**, *69*, 62.
(35) Cordero, B.; Gomez, V.; Platero-Prats, A. E.; Reves, M.; Echeverria, J.; Cremades, E.; Barragan, F.; Álvarez, S. *Dalton Trans.* **2008**, 2832–2838.
(36) Brisdon, A. K. *Inorganic Spectroscopic Methods*; Evans, J., Ed.; Oxford University Press, 1998; Vol. 62.
(37) SCM. *Amsterdam Density Functional, ADF* **2006**.
(38) Vosko, S. H.; Wilk, L.; Nusair, M. *Can. J. Phys.* **1980**, *58*, 1200-1211
(39) Becke, A. *Phys. Rev., A* **1988**, *38*, 3098–3100.
(40) Perdew, J. P. *Phys. Rev. B* **1986**, *33*, 8822–8824.
(41) Perdew, J. P. *Phys. Rev. B* **1986**, *34*, 7406–7406.
(42) Frisch, M.; Trucks, G. W.; Schlegel, H. B.; Scuseria, G. E.; Robb, M. A.; Cheeseman, J. R.;

Scalmani, G.; Barone, V.; Mennucci, B.; Petersson, G. A.; others. Gaussian 09, revision A. 02; Gaussian. *Inc., Wallingford, CT*, 2009, *270*, 271.
(43) Bain, G. A.; Berry, J. F. *J. Chem. Educ.* **2008**, *85*, 532-536.
(44) Coles, S. J.; Gale, P. A. *Chem. Sci.* **2012**, *3*, 683–689.
(45) Rigaku. *CrystalClear* **2011**.
(46) Agilent Technologies. *CrysalisPro 1.171.36.32* **2011**.
(47) Blessing, R. H. *Acta Crystallogr., A, Found. Crystallogr.* **1995**, *51*, 33–38.
(48) Sheldrick, G. M. *Acta Crystallogr., A, Found. Crystallogr.* **2008**, *64*, 112–122.
(49) Dolomanov, O. V.; Bourhis, L. J.; Gildea, R. J.; Howard, J. A. K.; Puschmann, H. *J. Appl. Crystallogr.* **2009**, *42*, 339–341.
(50) Farrugia, L. J. *J. Appl. Crystallogr.* **1999**, *32*, 837–838.